Dark Localized Waves in Shallow Waters: Analysis within an Extended Boussinesq System

Zhengping Yang[1], Wei-Ping Zhong[2,3*], and Milivoj Belić[3]

[1]*Department of Medical Science, Shunde Polytechnic, Shunde 528300, China*
[2]*Department of Electronic Engineering, Shunde Polytechnic, Shunde 528300, China*
[3]*Division of Arts and Sciences, Texas A & M University at Qatar, 23874 Doha, Qatar*

(Received 4 February 2024; accepted manuscript online 29 February 2024)

We study dark localized waves within a nonlinear system based on the Boussinesq approximation, describing the dynamics of shallow water waves. Employing symbolic calculus, we apply the Hirota bilinear method to transform an extended Boussinesq system into a bilinear form, and then use the multiple rogue wave method to obtain its dark rational solutions. Exploring the first- and second-order dark solutions, we examine the conditions under which these localized solutions exist and their spatiotemporal distributions. Through the selection of various parameters and by utilizing different visualization techniques (intensity distributions and contour plots), we explore the dynamical properties of dark solutions found: in particular, the first- and second-order dark rogue waves. We also explore the methods of their control. The findings presented here not only deepen the understanding of physical phenomena described by the (1+1)-dimensional Boussinesq equation, but also expand avenues for further research. Our method can be extended to other nonlinear systems, to conceivably obtain higher-order dark rogue waves.

DOI: 10.1088/0256-307X/41/4/044201

1. Introduction. As researchers delve deeper into research of little-known dynamical phenomena in the ocean, explorers have noticed the appearance of strange large-amplitude waves on the ocean surface, with heights exceeding 3–4 times the background water waves.[1] These waves, often described as "coming without a shadow, going without a trace",[2] appear with towering crests and plunging troughs, possessing the potential for devastating impact. Referred to as rogue waves (RWs),[1,2] they are alternatively labeled as giant waves, strange waves, killer waves, monster waves, or extreme waves.[3] At first, knowledge of these phenomena stemmed primarily from the anecdotal statements by ships' crews, lacking accurate measured data. Consequently, the understanding of giant waves was limited, receiving insufficient scientific attention for a long time.[1,3] However, with advancements in science and technology, ocean probes began observing the instances of RWs, such as the notable "New Year wave", detected in the North Sea.[4] This was also the first time that a giant wave was scientifically recognized as a challenging problem within the research community. After Draper first proposed the concept of RWs in 1964,[5] scholars from diverse disciplines, including oceanography, physics, and nonlinear sciences, increasingly focused their attention on this phenomenon and actively studied it from different perspectives. These included investigations into the modulation instability of nonlinear systems,[2] mechanisms of linear and nonlinear wave interaction,[6] and explorations of nonlinear optical systems.[7] A comprehensive overview of optical RWs and extreme events, together with their developmental pathways, was provided in a seminal "roadmap paper" published in 2016.[8]

More recently, a comprehensive theory of RWs has emerged, producing tremendous progress in nonlinear sciences, spanning disciplines such as nonlinear optics, plasma physics, cold atom condensates, and atmospheric science.[1] Researchers have successively observed RW phenomena in various controlled environments, including "optical rogue waves", "water tank rogue waves", and "plasma rogue waves" in the laboratory, thus providing strong support for RW research and inspiring researchers' enthusiasm for the new field.[7] Further investigations into RW patterns have unveiled their inherent structural complexity; in addition to the common basic structures of "nasal-eyes shape" and "four-petal shape", researchers have identified a myriad of other RW structures.[9] Notably, Akhmediev *et al.* introduced a rational fraction form to describe higher-order RWs of the classical nonlinear Schrödinger (NLS) equation, which can be understood as nonlinear superpositions of the first-order RWs.[10] They described the structure of higher-order giant waves as emergent from the collision of breathers, with distinct classifications for various structural configurations. Still, the structure of higher-order RWs is very complex, with many unresolved issues pertaining to the mechanisms underlying their formation.[11–16] Solving nonlinear models is another way to understand the formation of RWs and to explore other directions of their development. The research on rogue wave solutions of integrable nonlinear systems has become a current research hot spot.[1,3] RWs are heralded as a novel frontier within nonlinear science, akin to the revolutionary impact of solitons, signifying another trans-

*Corresponding author. Email: zhongwp6@126.com
© 2024 Chinese Physical Society and IOP Publishing Ltd

formative "nonlinear revolution" within the realm of localized waves.

Not surprisingly, at present, various new methods for treating solitons in different nonlinear evolution equations continue to emerge. The latest development uses deep learning techniques to such an end. For example, Xu *et al.* used physics-informed neural networks (PINNs) to solve the (1 + 1)-dimensional coupled nonlinear Schrödinger–Maxwell–Bloch equation,[17] while Liu *et al.* applied a similar neural network method to the NLS equation with party-time symmetric potentials.[18] Similarly, Wen *et al.* employed an extended PINN with twin subnets to study the coupled mixed-derivative NLS equation.[19] In contrast, Wang *et al.* used a bilinear method to obtain the two-soliton solution of the higher-order coupled NLS equation with variable coefficients.[20]

In 1871, Boussinesq introduced a groundbreaking nonlinear shallow water wave model,[21] capable of simulating an array of wave propagation phenomena that included shallow water deformation, reflection, diffraction, refraction, nonlinear wave interaction, wave fragmentation and dissipation, wave–current interaction, and wave-induced tidal currents.[22] As the utilization of the Boussinesq wave model proliferated across diverse fields, numerous scholars proposed various improvements to the Boussinesq equation to enhance its effectiveness. Zhu, for instance, applied the Dbar method to obtain the line and bright rational solutions of the Boussinesq equation.[22] Cao *et al.*[23] used the traveling wave assumption to obtain the bright and dark soliton solutions of the Boussinesq equation, and then applied the Hirota bilinear method to construct the N-order soliton and the N-order respiratory soliton solution of the Boussinesq equation. Building on this basis, Cao further derived the W-shaped linear strange wave solution, the single wave solution, a rational solution, and an interaction solution with the single wave, obtained using the long-wave limit method. Despite these strides, the special structures within an extended Boussinesq system (BS) introduced in this paper, namely the specific first-order and second-order dark rogue wave solutions, have not yet been reported in this form, to the best of our knowledge. In this work, we derive dark rational solutions using the multiple rogue wave method and explore ways to control them. One of the major motivations of this article is to extend the method to other nonlinear systems. These tasks constitute the primary focus of the present article.

The paper is structured as follows. In Section 2, we transform the extended BS into its bilinear form, utilizing the Hirota method. Then, with the help of symbolic calculus and the multiple rogue wave method, we derive the first- and second-order dark rational solutions. We examine the conditions governing the existence of localized RWs and their dynamic properties. In Section 3, we select specific model parameters to display spatiotemporal distributions of these solutions. We further discuss their sudden appearance and disappearance over time. Such transient behavior of dark RWs reflects the ephemeral nature of rogue waves and reveals some of their strange characteristics. Finally, we summarize our results in Section 4 and draw some insightful conclusions.

2. The Extended Boussinesq System and its Rational Dark Rogue Wave Solutions. The famous BS is a type of nonlinear system that describes dispersion and nonlinearity in shallow water waves. Its dispersion relation encompasses the dispersion phenomena observed in shallow water, nonlinear long waves, and Stokes waves. Accordingly, it has been widely applied in various fields, ranging from the modeling of water wave motion to the prediction of early gas behavior and marine environmental protection.[24,25] This article considers an extended (1+1)-dimensional dimensionless BS of the form:

$$\frac{\partial^2 u}{\partial t^2} - \frac{\partial^2 u}{\partial x^2} - \gamma \frac{\partial^4 u}{\partial x^4} - 3\chi \frac{\partial^2 u^2}{\partial x^2} = 0, \tag{1}$$

in which the wave packet $u(x,\, t)$ is a function of the dimensionless evolution time t and the dimensionless position coordinate x. Here, γ and χ are two arbitrary non-zero real constants. System (1) has been widely used in the analysis of long waves in shallow water and the analysis of water permeability in porous materials on the surface.[21,24,25]

To obtain the dark rogue wave solution of Eq. (1), we perform the well-known transformation of the wave packet:

$$u(x,\, t) = u_0 + 2\frac{\partial^2}{\partial x^2} \ln f, \tag{2}$$

where $u_0\,(\neq 0)$ is the background intensity (a real constant), $f = f(x,\, t)$ is an auxiliary function introduced to obtain the dark RW solution of system (1), generally playing an important role in treatments of various Boussinesq equations, as well as in this article. In particular, we find that system (1) can be described by the following Hirota bilinear form:

$$\left[D_t^2 - (1 + 6\chi u_0)\, D_x^2 - \gamma D_x^4\right] f \cdot f = 0, \tag{3}$$

where $u_0 \neq -1/6\chi$ and D is the Hirota operator, defined as[26,27]

$$D_x^m D_y^n \left[g\,(x,\, y) \cdot f\,(x, y)\right] = \left(\frac{\partial}{\partial x} - \frac{\partial}{\partial x'}\right)\left(\frac{\partial}{\partial y} - \frac{\partial}{\partial y'}\right) \times g\,(x,\, y)\, f\,(x, y)\Big|_{x=x',\, y=y'},$$

in which $g\,(x,\, y)$ and $f\,(x,\, y)$ are infinitely differentiable functions of $(x,\, y)$.

To obtain the general dark RW solution of Eq. (1), we use the multiple rogue wave method[24] to obtain its dark solutions, assuming that they are of the following form:[28]

$$f = F_{n+1}(x,\, t) + 2\alpha x P_n(x,\, t) + 2\beta t Q_n(x,\, t) + \left(\alpha^2 + \beta^2\right) F_{n-1}(x,\, t), \tag{4}$$

with

$$F_n(x,\, t) = \sum_{k=0}^{n(n+1)/2} \sum_{i=0}^{k} a_{n(n+1)-2k,2i}\, t^{n(n+1)-2k} x^{2i},$$

$$P_n(x,\, t) = \sum_{k=0}^{n(n+1)/2} \sum_{i=0}^{k} b_{n(n+1)-2k,2i}\, t^{n(n+1)-2k} x^{2i},$$

$$Q_n(x,\, t) = \sum_{k=0}^{n(n+1)/2} \sum_{i=0}^{k} c_{n(n+1)-2k,2i}\, t^{n(n+1)-2k} x^{2i},$$

where the initial terms are $F_0 = 1$ and $F_{-1} = P_0 = Q_0 = 0$. Here, $a_{m.l}$, $b_{m.l}$, $c_{m.l}$ are undetermined coefficients with

$m, l \in \{0, 2, 4, \ldots, n(n+1)/2\}$, and α and β are two arbitrary real constants. By substituting Eq. (4) into Eq. (3), the general expression for f is obtained. Then, using Eq. (2), the dark RW solutions of Eq. (1) are generated. Of special importance in our method is the fact that these RWs are localized in both x and t, which is the defining property of any solitary wave. This and other properties of dark RWs will be discussed below.

2.1. The First-Order Dark Rogue Wave Solution. In Eq. (4), by considering the case of $n = 0$ we will obtain the first-order dark RW solution of Eq. (1), whose basic form is

$$f = F_1(x, t) + 2\alpha x P_0(x, t) + 2\beta t Q_0(x, t) + \left(\alpha^2 + \beta^2\right) F_{-1}(x, t). \tag{5}$$

When $F_{-1} = P_0 = Q_0 = 0$, then

$$f(x, t) = F_1(x, t) = (t - \alpha)^2 + a_{0,2}(x - \beta)^2 + a_{0,0}, \tag{6}$$

where $a_{0,2} \neq 0$ and $a_{0,0} \neq 0$. By directly substituting Eq. (6) into the bilinear Eq. (3) and performing symbolic calculations using Mathematica software, one obtains a polynomial system. By solving this system of equations, one further obtains the values of constants in Eq. (6)

$$a_{0,0} = \frac{3\gamma}{(1 + 6\chi u_0)^2}, \tag{7}$$

$$a_{0,2} = -\frac{1}{1 + 6\chi u_0}, \tag{8}$$

where $u_0 \neq -1/6\chi$. Therefore, we obtain the expression for the auxiliary function,

$$f(x, t) = f_1(x, t) = (t - \alpha)^2 - \frac{1}{1 + 6\chi u_0}(x - \beta)^2 + \frac{3\gamma}{(1 + 6\chi u_0)^2}.$$

Using Eq. (2), one then obtains the first-order rational dark rogue wave solution of system (1),

$$u_1(x, t) = u_0 + \frac{4}{(1 + 6\chi u_0)^3} \frac{\left[(1 + 6\chi u_0)(x - \beta)^2 + (1 + 6\chi u_0)^2 (t - \alpha)^2 + 3\gamma\right]}{\left[(t - \alpha)^2 - \frac{1}{1 + 6\chi u_0}(x - \beta)^2 + \frac{3\gamma}{(1 + 6\chi u_0)^2}\right]^2}. \tag{9}$$

To ensure that Eq. (9) does not exhibit singularities, which means its denominator is never zero, it must be taken that $1 + 6\chi u_0 < 0$ and $\gamma > 0$. This, we believe, is a new dark rational RW solution of BS (1). We will elaborate on the specific examples in the next section.

2.2. The Second-Order Dark Rogue Wave Solution. We proceed, analogously, to obtain the second-order RW solution of Eq. (1). When $n = 1$, from Eq. (4) one finds that

$$f = F_2(x, t) + 2\alpha x P_1(x, t) + 2\beta t Q_1(x, t) + \left(\alpha^2 + \beta^2\right) F_0(x, t), \tag{10}$$

with

$$F_2(x, t) = t^6 + a_{4,0}t^4 + a_{4,2}t^4x^2 + \left(a_{2,0} + a_{2,2}x^2 + a_{2,4}x^4\right)t^2 + a_{0,0} + a_{0,2}x^2 + a_{0,4}x^4 + a_{0,6}x^6,$$

$$P_1(x, t) = b_{0,0} + b_{0,2}t^2 + b_{2,0}x^2,$$

$$Q_1(x, t) = c_{0,0} + c_{0,2}x^2 + c_{2,0}t^2,$$

$$F_0(x, t) = 1.$$

Namely,

$$\begin{aligned} f(x, t) &= f_2(x, t) \\ &= t^6 + a_{4,0}t^4 + a_{4,2}t^4x^2 + a_{2,0}t^2 + a_{2,2}x^2t^2 \\ &\quad + a_{2,4}x^4t^2 + a_{0,0} + a_{0,2}x^2 + a_{0,4}x^4 + a_{0,6}x^6 \\ &\quad + 2\alpha b_{0,0}x + 2\alpha b_{0,2}xt^2 + 2\alpha b_{2,0}x^3 + 2\beta c_{0,0}t \\ &\quad + 2\beta c_{0,2}x^2t + 2\beta c_{2,0}t^3 + \alpha^2 + \beta^2. \end{aligned} \tag{11}$$

Substituting Eq. (11) into Eq. (3), and assuming the coefficients of the same power of $x^l t^k$ ($l = 0, 1, 2, \ldots$, $k = 0, 1, 2, \ldots$) to all be zero, we generate a complex polynomial system. Again, by performing symbolic calculations using Mathematica, we obtain specific solutions. Note that $a_{0,0}$, $b_{0,0}$, and $c_{0,0}$ are not completely independent; when selecting $b_{0,0}$ and $c_{0,0}$ as independent variables, other parameters can be expressed as

$$a_{4,0} = \frac{17\gamma}{(1 + 6\chi u_0)^2}, \quad a_{4,2} = -\frac{3}{1 + 6\chi u_0}, \tag{12}$$

$$a_{2,0} = \frac{475\gamma^2}{(1 + 6\chi u_0)^4}, \quad a_{2,2} = -\frac{90\gamma}{(1 + 6\chi u_0)^3},$$

$$a_{2,4} = \frac{3}{(1 + 6\chi u_0)^2}, \tag{13}$$

$$a_{0,0} = \frac{1875\gamma^3}{(1 + 6\chi u_0)^6} - \left(\alpha^2 + \beta^2\right) + \frac{(1 + 6\chi u_0)^4}{25\gamma^2}\beta^2 c_{0,0}^2 - \frac{(1 + 6\chi u_0)^5}{\gamma^2}\alpha^2 b_{0,0}^2, \tag{14}$$

$$a_{0,2} = \frac{125\gamma^2}{(1 + 6\chi u_0)^5}, \quad a_{0,4} = \frac{25\gamma}{(1 + 6\chi u_0)^4},$$

$$a_{0,6} = -\frac{1}{(1 + 6\chi u_0)^3}, \tag{15}$$

$$b_{0,2} = \frac{3(1 + 6\chi u_0)^2}{\gamma} b_{0,0}, \quad b_{2,0} = \frac{1 + 6\chi u_0}{\gamma} b_{0,0}, \tag{16}$$

$$c_{0,2} = -\frac{3(1 + 6\chi u_0)}{5\gamma} c_{0,0}, \quad c_{2,0} = -\frac{(1 + 6\chi u_0)^2}{5\gamma} c_{0,0}. \tag{17}$$

Using Eq. (2), one can then generate a second-order dark RW solution of system (1), which is generally expressed as

$$u_2(x, t) = u_0 + 2\frac{\partial^2}{\partial x^2} \ln f_2, \tag{18}$$

where $f_2(x, t)$ is determined by Eq. (11), and the various coefficients of $f_2(x, t)$ by Eqs. (12)–(17); and, of course, $b_{0,0} \neq 0$, $c_{0,0} \neq 0$. As long as one selects the appropriate parameters $b_{0,0}$ and $c_{0,0}$, various second-order dark RW solutions will be generated, which is an interesting possibility that will be further explored in the next section.

3. The Dynamic Behavior of Dark Rogue Waves. In the above section, we obtained dark RW solutions of the BS (1). Based on these solutions, we will select appropriate parameters, to study their dynamic behavior and the methods of control.

3.1. The Dynamic Behavior of First-Order Dark Rogue Waves. As an example, by selecting $u_0 = 3$, $\gamma = 1$, $\chi = -1/9$, $1 + 6\chi u_0 = -1$, after simple algebraic calculations, Eq. (9) can be rewritten as the following rational expression:

$$u_1(x, t) = 3 + \frac{4\left[(t-\alpha)^2 - (x-\beta)^2 + 3\right]}{\left[(t-\alpha)^2 + (x-\beta)^2 + 3\right]^2}. \tag{19}$$

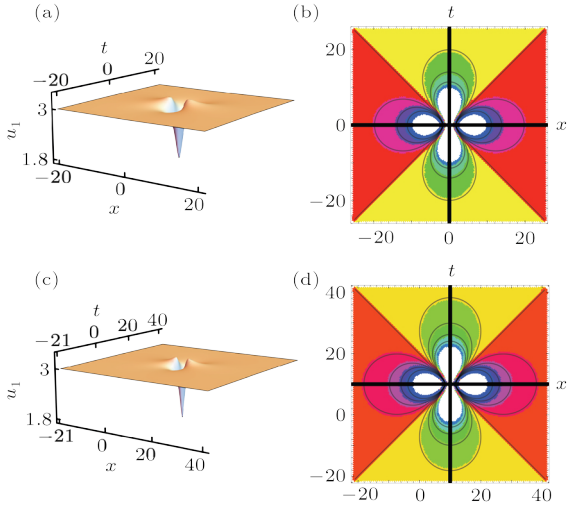

Fig. 1. Profiles of the first-order dark RW with the parameters $u_0 = 3$, $\gamma = 1$, $\chi = -1/9$ in Eq. (19). Upper row: RW centered at the (0, 0) point. Lower row: RW centered at the (10, 10) position. Other parameters are provided in the text.

Note that the denominator of the analytical expression (9) cannot be zero: so when $1 + 6\chi u_0 < 0$ and $\gamma > 0$, $u_1(x, t)$ is a nonsingular wave packet. By performing extreme value analysis on $u_1(x, t)$, it can be ascertained that the position of the trough of this dark RW (i.e., the center position of the first-order dark rogue wave) is $(x, t) = (\beta, \alpha)$. Figure 1 depicts its basic characteristics. On the left is the three-dimensional profile with the vertical direction representing $u_1(x, t)$, and on the right is the corresponding contour plot. We select $(\beta, \alpha) = (0, 0)$ for the top row and $(\beta, \alpha) = (10, 10)$ for the bottom row. From Fig. 1, it is observed that the first-order dark RW is a localized wave packet with three peaks, whose two side peaks are above the background intensity and the middle peak is below the background intensity. The pair of physical parameters (α, β) for this type of dark rogue wave represent its controlled center. The energy is concentrated near the center point $(x, t) = (\beta, \alpha)$.

To graphically demonstrate that the center position of this first-order dark RW solution is indeed at $(x, t) = (\beta, \alpha)$, we first select $\beta = 0$ and $\alpha = 10$. The upper row of Fig. 2 exhibits the dynamic behavior under these specific parameters. At this point, the center of the first-order dark RW is located at position $x = \beta$ on the x-axis. In another case, we select $\beta = 10$ and $\alpha = 0$, and the lower row of Fig. 2 shows its spatiotemporal distribution. The center position is displaced on the t-axis, at $t = 10$. It is obvious that the positions of the two peaks (greater than the background intensity) are located on the same straight line, and the positions of the two peaks are symmetric about the position of the valley (which is lower than the background intensity). Thus, α and β only control the position of dark RWs, without affecting their peak and trough values.

In Figs. 1 and 2, one can observe the characteristics of the first-order dark RWs. Firstly, they are spatiotemporally localized, and display a structure that is similar to the inverted bright rogue waves.[12–15] The second characteristic is that there is "no shadow and no trace"; there is a sudden peak appearing and disappearing fast. The third is that the energy is concentrated in a very small area and, consequently, the wave may possess great destructive power.

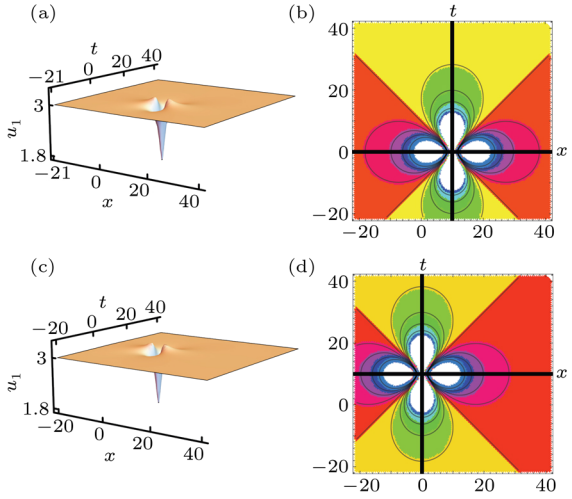

Fig. 2. Profiles of the first-order dark rogue wave with the center position drift. The setting is the same as in Fig. 1, except for the values of position parameters α and β.

3.2. The Dynamic Behavior of Second-Order Dark RWs. As is evident from the second-order dark RW solution (18), its expression is quite complex. There are four independent parameters; in addition to α and β, there are two other parameters $b_{0,0}$ and $c_{0,0}$. When selecting $b_{0,0} = c_{00} = 0.6$ and $\alpha = \beta = 0$, and (similar to the first-order dark RWs) other parameters as $u_0 = 3$, $\gamma = 1$, $\chi = -1/9$ in Eqs. (11) and (18), the upper row of Fig. 3 displays the dynamic behavior of the second-order dark RW solution. It exhibits three peaks (greater than the background intensity) and two valleys (lower than the background intensity); the wave packet in the middle position is the largest, and the main energy is concentrated at the $(x, t) = (0, 0)$ position. Three peaks are located on the t-axis, while the other two valleys are on the x-axis (see the contour plot). The secondary peaks and two valleys display a high degree of symmetry, all centered around $(x, t) = (0, 0)$. This symmetry is lost when parameters α and β take nonzero values; for large values,

the second-order dark RWs gradually separate and form three first-order dark RWs. The lower row of Fig. 3 shows the spatiotemporal distribution of the second-order dark RWs when the parameters are $\alpha = 50$, $\beta = 30$, and other parameters are the same as in the upper row. The amplitudes of these three wave packets are different and possess no specific symmetry.

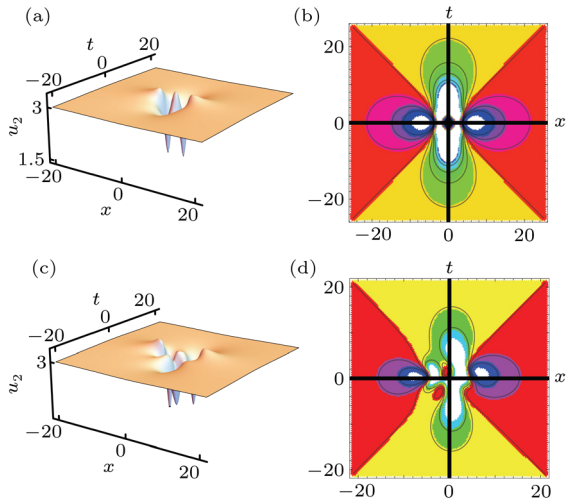

Fig. 3. Profiles of the second-order dark rogue wave with the parameters $u_0 = 3$, $\gamma = 1$, $\chi = -1/9$ in Eq. (18). Other parameters are provided in the text. Upper row: a symmetric dark RW for $\alpha = \beta = 0$. Lower row: an asymmetric dark RW with the nonzero values of $\alpha = 50$, $\beta = 30$.

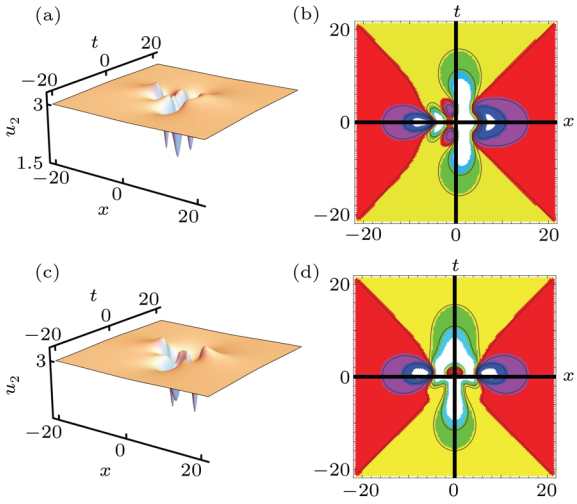

Fig. 4. Profiles of the second-order dark rogue wave with different α and β. The setting is the same as in Fig. 3, except for the values of parameters α and β.

Next, we demonstrate the second-order dark rogue wave patterns of solution (18) for different values of parameters α and β. Under the same parameters as in the upper row of Fig. 3, we only change α and β to explore the dynamic behavior of second-order dark RWs. When $\alpha = 50$ and $\beta = 0$ are selected, the upper row of Fig. 4 shows the spatiotemporal distribution. The wave is still composed of three first-order dark RWs, which display no symmetry at all. When the same parameter values are selected, $\alpha = \beta = 50$, the distribution is displayed in the lower row of Fig. 4. From its contour plot, it can be observed that the wave packet obeys a mirror symmetry about the t-axis.

From the above analysis, one can conclude that as long as $\alpha \neq 0$ or $\beta \neq 0$, the second-order dark RW consists of three first-order dark RWs. Selecting $\alpha = \beta \neq 0$ (none of which are zero), the wave packet exhibits mirror symmetry about the t-axis. The center position of this second-order RW is independent of α and β.

4. Conclusions. We have investigated the $(1 + 1)$-dimensional BS, using the Hirota bilinear form and the multiple rogue wave method. With the help of Mathematica software and symbolic calculations, we derive the first- and second-order dark RW solutions of the system. Based on these exact dark RW solutions, the controlled behavior of the BS is further studied.

By selecting appropriate system parameters and discussing the method for control of dark RWs, such as controlling the center position of the first- and second-order dark EWs, a degree of control of these waves is achieved. Research has shown that in addition to the unpredictable characteristics of "coming without shadow and going without trace," these dark RWs exhibit controllable properties; that is, by selecting suitable parameters, the behavior of the dark RW can be reasonably well controlled.

These results may lay a theoretical foundation for the hazard avoidance and dynamical control of dark RWs. They also possess potential application value for the controlled propagation of dark RWs in nonlinear media. The third-order and higher-order dark RW solutions require further exploration in the future. The method for finding dark rogue waves of the BS used in this study can be extended to other nonlinear systems.

Acknowledgements. This work was supported by the National Natural Science Foundation of China (Grant No. 62275176), the Natural Science Foundation of Guangdong Province, China (Grant No. 2022A1515010084), and Key projects of basic research and applied basic research in universities of Guangdong province, China (Grant Nos. 2021ZDZX1118 and 2022ZDZX1079). The work at the Texas A&M University at Qatar was supported by the NPRP 13S-0121-200126 project with the Qatar National Research Fund (a member of Qatar Foundation).

References

[1] Akhmediev N, Dudley J M, Solli D R, and Turitsyn S K 2013 *J. Opt.* **15** 060201

[2] Akhmediev N, Soto-Crespo J M, and Ankiewicz A 2009 *Phys. Lett. A* **373** 2137

[3] Kharif C and Pelinovsky E 2003 *Eur. J. Mech.* **22** 603

[4] Walker D A G, Taylor P H, and Taylor R E 2004 *Appl. Ocean Res.* **26** 73

[5] Draper L 1964 *Oceanus* **10** 13

[6] Zakharov V E, Dyachenko A I, and Prokofiev A O 2006 *Eur. J. Mech.* **25** 677

[7] Solli D R, Ropers C, Koonath P, and Jalali B 2007 *Nature* **450** 1054

[8] Akhmediev N, Kibler B, Baronio F *et al.* 2016 *J. Opt.* **18** 063001

[9] Zhong W P, Belić M, and Huang T 2013 *Phys. Rev. E* **87** 065201
[10] Akhmediev N, Ankiewicz A, and Soto-Crespo J M 2009 *Phys. Rev. E* **80** 026601
[11] Zhong W P, Chen L, Belić M, and Petrović N 2014 *Phys. Rev. E* **90** 043201
[12] Kedziora D J, Ankiewicz A, and Akhmediev N 2013 *Phys. Rev. E* **88** 013207
[13] Yang J and Zhu Y 2023 *Phys. Lett. A* **487** 129117
[14] Zhong W P, Belić M, and Malomed B A 2015 *Phys. Rev. E* **92** 053201
[15] Sun W R and Liu M M 2022 *Phys. Lett. A* **456** 128539
[16] Yang Z P, Zhong W P, Belić M, and Zhang Y Q 2018 *Opt. Express* **26** 7587
[17] Xu S Y, Zhou Q, and Liu W 2023 *Nonlinear Dyn.* **111** 18401
[18] Liu X M, Zhang Z Y, and Liu W J 2023 *Chin. Phys. Lett.* **40** 070501
[19] Wen X K, Jiang J H, Liu W, and Dai C Q 2023 *Nonlinear Dyn.* **111** 13343
[20] Wang S B, Ma G L, Zhang X, and Zhu D Y 2022 *Chin. Phys. Lett.* **39** 114202
[21] Boussinesq J 1871 *Comptes Rendus de l' Academie des Sciences* **72** 755
[22] Zhu J Y 2017 arXiv:1704.02779 [nlin.SI]
[23] Cao Y L, He J S, and Mihalache D 2018 *Nonlinear Dyn.* **91** 2593
[24] Ma W X, Li C X, and He J 2009 *Nonlinear Analysis* **70** 4245
[25] Wazwaz A M 2008 *Appl. Math. Comput.* **203** 277
[26] Hirota R 1973 *J. Math. Phys.* **14** 805
[27] Zhong W P, Belić M, Assanto G, Malomed B A, and Huang T 2011 *Phys. Rev. A* **84** 043801
[28] Clarkson P A and Dowie E 2017 *Trans. Math. Its Appl.* **1** tnx003